



ST-ECF Instrument Science Report WFC3-2009-18

# WFC3 SMOV proposal 11552: Calibration of the G102 grism

H. Kuntschner, H. Bushouse, M. Kümmler, J. R. Walsh  
October 16, 2009

---

## ABSTRACT

*Based on the SMOV observations, the performance of the WFC3 near-IR grism G102 has been assessed. The location of the +1<sup>st</sup> spectral order relative to the source positions in the direct imaging filters F098M and F105W are determined, field dependent trace and wavelength solutions are derived, and the absolute throughput is quantified. Similar information is derived for higher spectral orders and the -1<sup>st</sup> order. The trace and wavelength solutions were found to be linear functions, varying smoothly over the field of view. Generally, there is good agreement ( $\leq 1$  pixel) with the calibration solutions derived during the ground calibrations in TV2 and TV3.*

*For the +1<sup>st</sup> order aperture corrections are provided as a function of wavelength. The cross-dispersion PSF is evaluated and agrees with the design expectations as well as ground calibration measurements.*

*All calibrations in this ISR are given with respect to source positions derived from F098M images. Source positions obtained from F105W images show a systematic offset relative to F098M images of  $\Delta X = -0.135 \pm 0.002$  and  $\Delta Y = -0.250 \pm 0.002$  which needs to be corrected for when using the calibrations of this ISR.*

*The +1<sup>st</sup> order of the G102 grism shows a mean dispersion of 24.5 Å/pixel with a resolving power of  $R \sim 155$  at 10400 Å. The throughput of HST + WFC3 G102 peaks at 11000 Å with 41.8% and is above 10% between 8000 and 11500 Å.*

---

## 1. Introduction

The Wide Field Camera 3 (WFC3) is fitted with three gratings for slitless spectroscopy. In the UVIS channel there is one grating, G280, for the near-UV to visible range (200 - 400nm). The NIR channel has two gratings, G102 and G141, for the shorter (800 - 1150nm) and longer NIR wavelengths (1100-1700nm), respectively. The results from ground calibration efforts, including trace, wavelength, flat-field, throughput and aperture correction calibrations are summarized in Kuntschner et al. (2008a,b) and Kuntschner et al. (2009). This report presents the first in-orbit calibrations for the G102 grating derived from SMOV and selected Cycle 17 calibration observations.

## 2. Observations

The calibrations presented in this report are based on the SMOV program 11552 (PI: Bushouse), which comprises observations of the HST primary flux standard star GD153, and the wavelength calibrator planetary nebula HB12 (= PN G111.8-02.8) at several positions over the field-of-view (hereafter FoV). Furthermore, we made use of the Cycle 17 calibration program 11937 (PI: Bushouse), which comprises observations of the wavelength calibrator PN Vy2-2 over 9 different field positions. A summary of the pointing locations for all observations is given in Figure 1.

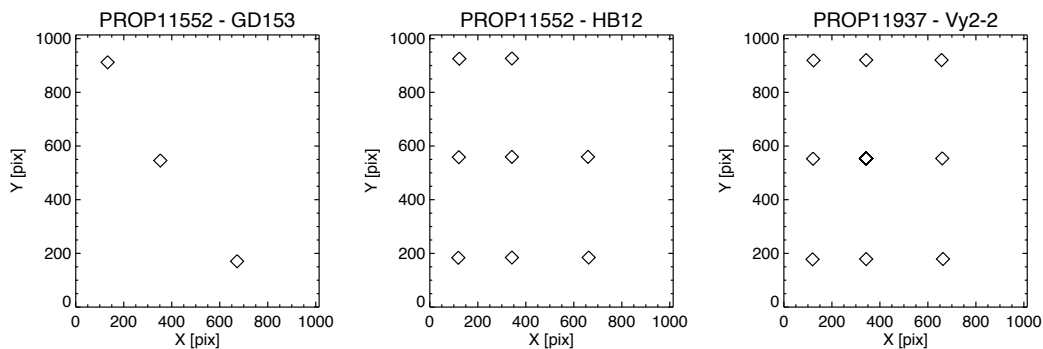


Figure 1: Distribution of target positions as seen on the F098M images for the SMOV proposal 11552 (GD153 and HB12) as well as Cycle 17 calibration proposal 11937 (Vy2-2).

For each position one or more G102 grating exposures were acquired. Due to a wrongly commanded POSTARG, one grating observation of HB12 (top right in the

central panel of Figure 1) was offset from the direct image position and is omitted from the analysis in this report. A detailed listing of all exposures used in this report is given in the Appendix.

### 3. Analysis

In this section we describe the analysis of the calibration data obtained for the G102 grism in proposals 11552 and 11937 yielding calibrations for the trace, the wavelength solution and the absolute throughput. Furthermore, we investigate offsets between the filters F098M and F105W. If not noted otherwise, analysis was carried out on fully processed images (i.e. "flt" files). The files were produced with the calwf3 pipeline, which carries out the basic data reductions including the following tasks:

- Flag known bad pixels in the data quality (DQ) array
- Subtract bias drifts determined from the reference pixels
- Identify pixels in the initial ("zeroth") read that contain detectable source signal
- Subtract the zeroth read
- Calculate a noise model for each pixel and record in the error (ERR) array
- Subtract dark image
- Correct for photometric non-linearity
- Convert the data to signal rates (DN per second)
- Perform "up-the-ramp" fitting and cosmic-ray rejection
- Perform flat-fielding and apply gain calibration (electrons per second)

The grism images are not flat-fielded with the normal procedure since for grism spectroscopy a given pixel can receive any wavelength for which the combination of camera and grism shows throughput. In our analysis we employ a special flat-field procedure where for each extracted pixel a wavelength dependent flat-field is applied; therefore calwf3 only applies the gain calibration to grism images. The grism flat-field information was determined during ground calibration and is stored in a flat-field cube (see Kuntschner et al 2008b).

In Figure 2 we show a typical direct image – G102 grism image pair by using observations of the flux standard star GD153.

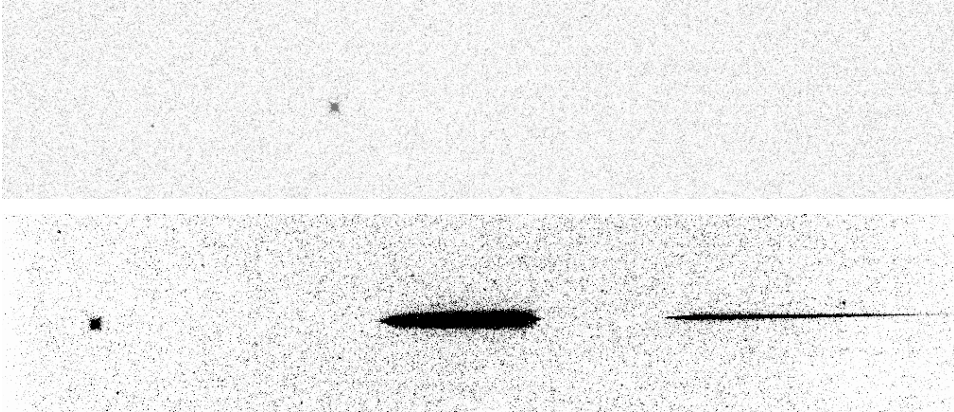
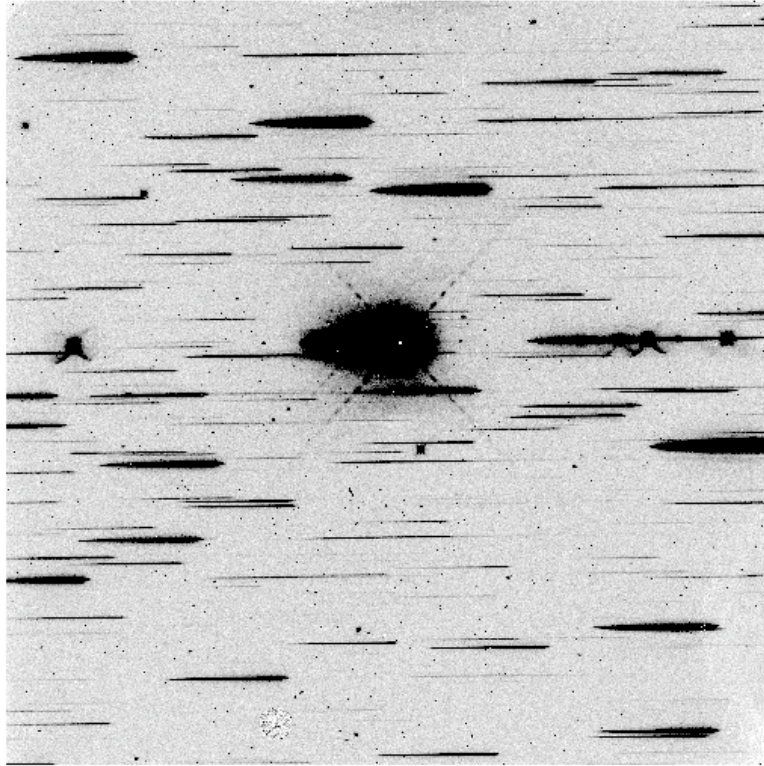


Figure 2: Example of a typical direct image – grism image pair for the G102 grism. The top panel shows a F098M image (*iab901eiqflt.fits*) of the flux standard GD153 and the bottom panel shows a G102 grism exposure (*iab901ekqflt.fits*) for the same region on the sky. The point like source on the left-hand side of the grism image is the zeroth order spectrum; the +1<sup>st</sup> and +2<sup>nd</sup> orders follow to the right. For each image we show the full extent of the detector in the x-direction and about 200 pixels in the y-direction.

### 3.1. Trace calibration

In order to establish a good in-orbit trace calibration, we utilize the G102 grism exposures of the PN HB12. For the trace calibration, we are not interested in the primary target itself but in the other point sources around the primary target. This field (galactic latitude: -02.8498 degrees) comprises a relatively good compromise between field coverage + object density and thus avoiding too much spectral overlap between different sources in the FoV (see Figure 2). The ST-ECF aXe software package for the reduction of slitless spectroscopy data treats the spectral traces and wavelength solutions defined with respect to the position of the source in the direct image. The centroids of all sources above a given threshold in the F098M images ( $X_{\text{ref}}$ ,  $Y_{\text{ref}}$ ) were determined with SExtractor (Bertin & Arnouts, 1996). These positions were assumed not to change between the observations of each direct image grism pair. The spectra of all sources were traced as a function of  $\Delta X = X - X_{\text{ref}}$  in the detector X-direction by measuring the centroids of 7-10 pixel wide bins, using custom-written IDL programs. We found the traces of all orders (excluding the zeroth order) to be well fit by straight lines with standard deviations of  $\leq 0.1$  pixels. The trace definitions are of the form  $(Y - Y_{\text{ref}}) = \text{DYDX}_0 + \text{DYDX}_1 * \Delta X$ , where  $\text{DYDX}_0$  and  $\text{DYDX}_1$  are field dependent and given in the usual format used by the ST-ECF aXe reduction package, e.g.,  $\text{DYDX}_1 = a0$

$+a1*X_{ref} + a2*Y_{ref} + \dots$  (see also the aXe manual<sup>1</sup> for more details).



*Figure 2: Image of the G102 grism exposure (iab907j6q\_ft.fits). The primary target HB12 is located in the centre. Most of the other prominent spectra are first orders of different (stellar) objects in the FoV used for the trace calibration.*

The final, field dependent trace solution for the +1<sup>st</sup> order of the G102 grism was derived from 137 different traces covering semi-uniformly the FOV. A graphical representation of the measured offsets and slopes as a function of  $X_{ref}$  and  $Y_{ref}$  positions is given in Figure 3. The offset shows a marked trend with  $Y_{ref}$  position while the slope shows a more complex dependence on  $X_{ref}$  and  $Y_{ref}$ . The offset is well represented with a field dependent fit using only a linear function (rms = 0.07 pixel), while the slope required a fit with quadratic terms (rms = 0.0004). The in-orbit calibrations show reasonably good agreement with the ground calibrations obtained in TV2 and TV3 with differences of  $\sim 0.3$  pixel in the offset and good

---

<sup>1</sup> [http://www.stecf.org/software/slitless\\_software/axe/](http://www.stecf.org/software/slitless_software/axe/)

agreement for the slope. The results of our field dependent fits are given in Table 1 and are also shown in Figure 3.

For the  $-1^{\text{st}}$ ,  $+2^{\text{nd}}$  and  $+3^{\text{rd}}$  orders a similar procedure was carried out, however, due to the reduced field coverage for these orders the field dependent fits were more restricted and the trace prediction accuracy is reduced. Results are summarized in Table 1. For the  $0^{\text{th}}$  order we adopt the trace determined in the ground calibrations.

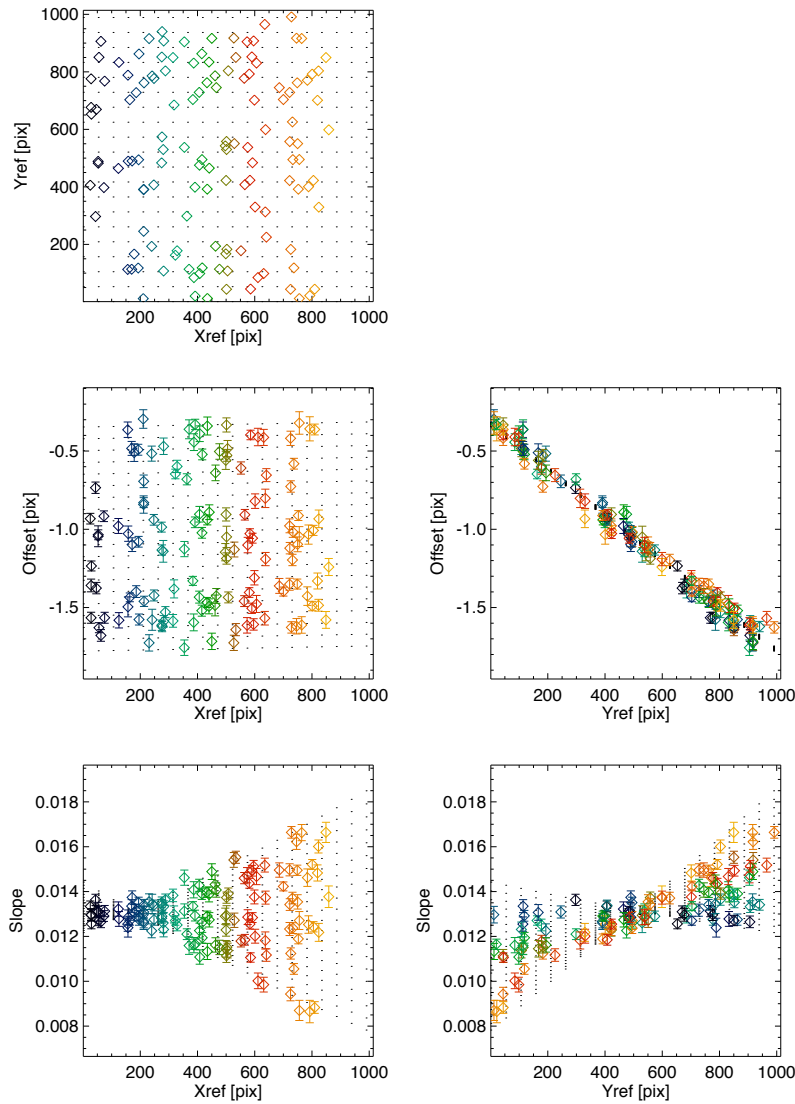


Figure 3: The trace fits for the G102  $1^{\text{st}}$  order spectra are shown as a function of  $X_{\text{ref}}$  and  $Y_{\text{ref}}$  position (diamond symbols). A total of 137 different source positions are used covering well the field-of-view (top left panel). The final field-dependent trace solution fit (see also Table 1) is shown as the grid of black dots.

**Table 1: Field dependent trace descriptions for G102. Where available errors are given below the values**

| Term                         | a0           | a1(X)        | a2(X)        | a3(X^2)     | a4(X*Y)     | a5(Y^2)     |
|------------------------------|--------------|--------------|--------------|-------------|-------------|-------------|
| <b>+1<sup>st</sup> order</b> |              |              |              |             |             |             |
| DYDX_A_0                     | -3.55018E-01 | 3.28722E-05  | -1.44571E-03 | -           | -           | -           |
| error                        | 7.40459E-02  | 4.44565E-06  | 3.65312E-06  | -           | -           | -           |
| DYDX_A_1                     | 1.42852E-02  | -7.20713E-06 | -2.42542E-06 | 1.18294E-09 | 1.19634E-08 | 6.17274E-10 |
| error                        | 3.86038E-04  | 4.21303E-07  | 3.42753E-07  | 4.26462E-10 | 3.51491E-10 | 3.02759E-10 |
| <b>0<sup>th</sup> order</b>  |              |              |              |             |             |             |
| DYDX_B_0                     | -3.65493E+00 | 8.44943E-04  | -1.18903E-03 | -           | -           | -           |
| DYDX_B_1                     | 0.0          | -            | -            | -           | -           | -           |
| XOFF_B                       | -2.59176E+02 | -1.71540E-03 | 1.50110E-02  | -           | -           | -           |
| YOFF_B                       | 0.0          | -            | -            | -           | -           | -           |
| <b>+2<sup>nd</sup> order</b> |              |              |              |             |             |             |
| DYDX_C_0                     | 4.91527E-01  | -2.41495E-04 | -3.22971E-03 | -           | -           | -           |
| error                        | 3.06620E-01  | 1.08980E-05  | 7.24872E-06  | -           | -           | -           |
| DYDX_C_1                     | 9.40642E-03  | -3.83750E-07 | 5.90327E-06  | -           | -           | -           |
| error                        | 9.48439E-04  | 1.85152E-07  | 1.03591E-07  | -           | -           | -           |
| <b>+3<sup>rd</sup> order</b> |              |              |              |             |             |             |
| DYDX_D_0                     | 1.86393E+00  | 0.0          | -6.43211E-03 | -           | -           | -           |
| error                        | 9.38073E-01  | -            | 6.23216E-05  | -           | -           | -           |
| DYDX_D_1                     | 5.67095E-03  | 0.0          | 1.16131E-05  | -           | -           | -           |
| error                        | 1.16444E-03  | -            | 1.36109E-06  | -           | -           | -           |
| <b>-1<sup>st</sup> order</b> |              |              |              |             |             |             |
| DYDX_E_0                     | -4.63065E-01 | 0.0          | -2.70816E-03 | -           | -           | -           |
| error                        | 8.79282E-02  | -            | 3.12092E-05  | -           | -           | -           |
| DYDX_E_1                     | 1.20848E-02  | 0.0          | -3.32426E-06 | -           | -           | -           |
| error                        | 1.22813E-04  | -            | 1.00255E-06  | -           | -           | -           |

Notes: The 0<sup>th</sup> order trace solutions are taken from the ground calibrations.

### 3.2. Position dependence on filter

The trace and wavelength calibrations reported in this ISR are based on the source positions measured from the standard filter F098M. An alternative filter for the G102 grism would be F105W. If the F105W filter introduces a shift in source pixel positions with respect to the F098M filter, the trace and wavelength calibrations are directly affected. We tested for these potential shifts by using the imaging of Proposal 11937 (PN Vy2-2). For each pair of F098M and F105W images taken at the same POSTARGS, we ran Sextractor and matched the source positions. In total

there are 9 image pairs, which yielded 828 matched object positions after some robust cleaning had been applied.

The resulting mean offsets were derived with a biweight mean estimator (IDL `biweight_mean.pro`) and are given in Table 2. The analysis showed little evidence for a field-position dependence of the shifts as can be seen from Figure 4. Using the mean shifts will result in a source position accuracy of  $<0.1$  pixel which is sufficient for the use of aXe.

**Table 2: Source position offsets between F098M and F105W**

|                      | <b>X offset [pixel]</b> | <b>Y offset [pixel]</b> |
|----------------------|-------------------------|-------------------------|
| <b>F098M – F105W</b> | <b>-0.135±0.002</b>     | <b>-0.250±0.002</b>     |



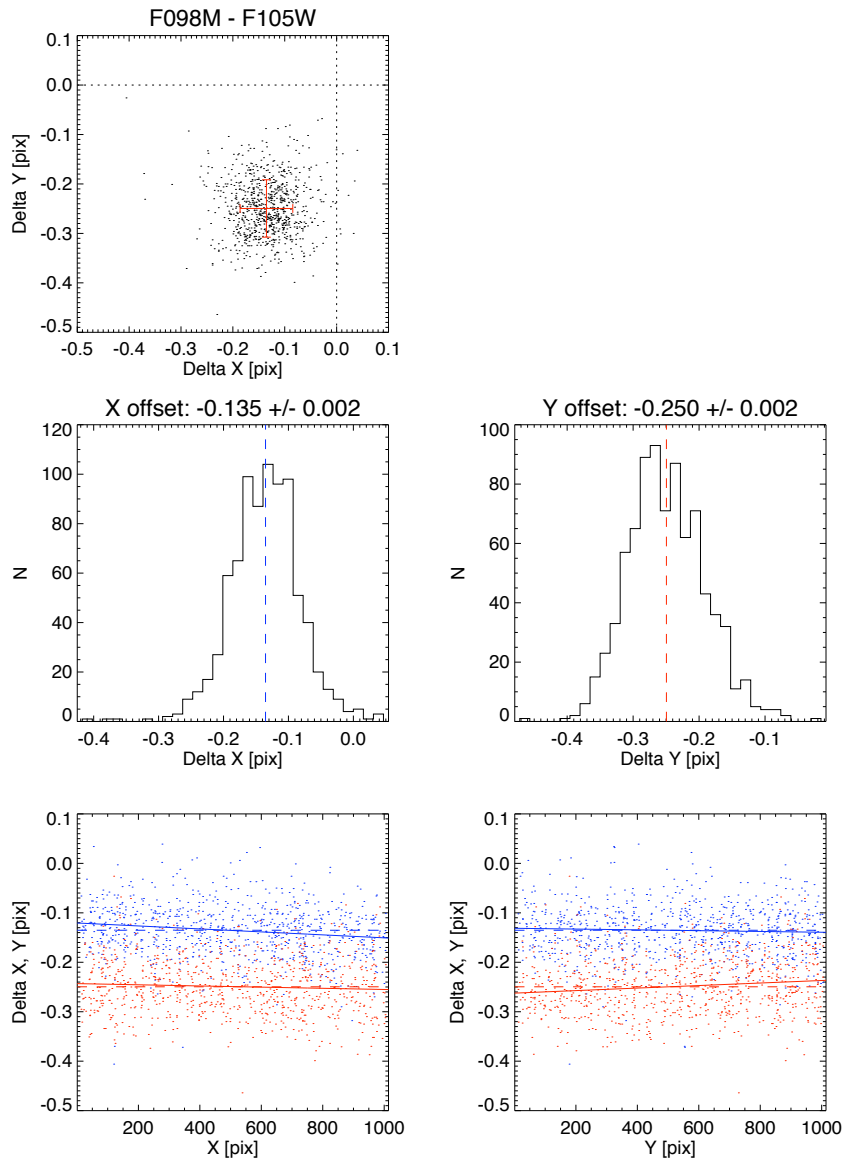


Figure 4: Source position shifts between the filters F098M and F105W. A total of 828 sources were matched in the direct imaging of Proposal 11937. Individual offsets and the mean are shown in the top panel. Histograms versus x and y-axis are shown in the middle panels whereas potential offset dependence with X and Y position is explored in the bottom panels. Solid lines show a robust linear fit, while the dashed lines indicate the mean shift in x (blue) and y (red).

### 3.3. Wavelength solutions

In order to establish the in-orbit wavelength calibration, the PN HB12 was observed during SMOV (Proposal 11552). Despite the extended nature of the object, the central pixels of the source saturate even in the first read of the direct image, which makes it difficult to determine an accurate source position. The PN Vy2-2 was observed as a wavelength calibrator as part of the Cycle 17 calibration program (Proposal 11937). This PN is somewhat fainter and accurate positions of the source could be derived from the direct imaging. However, also here the first read is slightly saturated and the final positions were derived from the zeroth read using the “\*\_raw.fits” files.

For wavelength calibration one would ideally want point sources with clearly identifiable emission lines over the wavelength range and at the resolution of the grism. While bright, nearby PNs do show a reasonably good distribution of emission lines, they are slightly extended at the spatial resolution of the WFC3 IR camera. Since the PNs Vy2-2 and HB12 have already been used for NICMOS grism calibration (see Pirzkal et al. 2009) and they offer a reasonable balance between brightness, number of emission lines and wavelength coverage, we opted for using those targets in the first wavelength calibrations of the WFC3 IR grisms. Future calibration programs may consider the use of e.g., WR stars or M-dwarfs.

Using the trace calibration described in Section 3.1 we extracted the spectra of Vy2-2 at all nine field positions with the help of the aXe software. In this extraction a special configuration file was used which provided spectra with counts versus pixel number along the x-axis. For the G102 grism a total of 9 emission features could be identified and used to establish the wavelength solution (see Table 3). Prior to the fitting, the radial velocity of -71 km/s for Vy2-2 and an air to vacuum conversion was applied to the tabulated wavelength of the emission lines (see Table 3). The ground calibration efforts suggested that a linear wavelength solution is a good representation of the true wavelength solution for this grism (Kuntschner et al. 2008a, b). Therefore we established for each spatial position a linear wavelength solution (see Figure 5) where fits give a typical rms scatter of 0.2-0.3 pixel (see Figure 5). The resulting wavelength solution shows typical errors of 5 Å for the zeropoint and 0.04 Å/pixel for the dispersion (~24.5 Å/pixel). Sometimes the emission lines are affected by e.g., cosmic ray hits, hot/dead pixels etc. and thus good emission line centroids could not be established. Therefore we used a 3-sigma rejection iteration for each linear fit to remove outliers. The He I line at 1083.03 nm is saturated in the data. However, we removed the saturated pixels from the fit and used the line wings to establish a fit to the line.

There is marginal evidence in the in-orbit data for a non-linear wavelength solution; however, the deviations appear to be <0.5 pixel over the full wavelength range (780 to 1100 nm). More wavelength calibration observations, including the use of true point sources, are needed to confirm any non-linear dispersion solution.

**Table 3: Rest air wavelength of emission features fitted to Vy2-2**

| Name     | Wavelength [ $\text{\AA}$ ] |
|----------|-----------------------------|
| [Ar III] | 7751.1                      |
| O I      | 8446.4                      |
| H P11    | 8862.8                      |
| [S III]  | 9068.6                      |
| H P9     | 9229.0                      |
| [S III]  | 9530.6                      |
| H P7     | 10049.4                     |
| [S II]   | 10321.9 <sup>2</sup>        |
| He I     | 10830.3                     |

---

<sup>2</sup> The rest wavelength of the [S II] emission line is 10328.9, however, a ground based spectrum of Vy2-2 (Hora et al. 1999) suggests that at the spectral resolution of the G102 grism the effective peak wavelength is reduced by  $\sim 7 \text{ \AA}$ . In the fits we used this adjusted value.

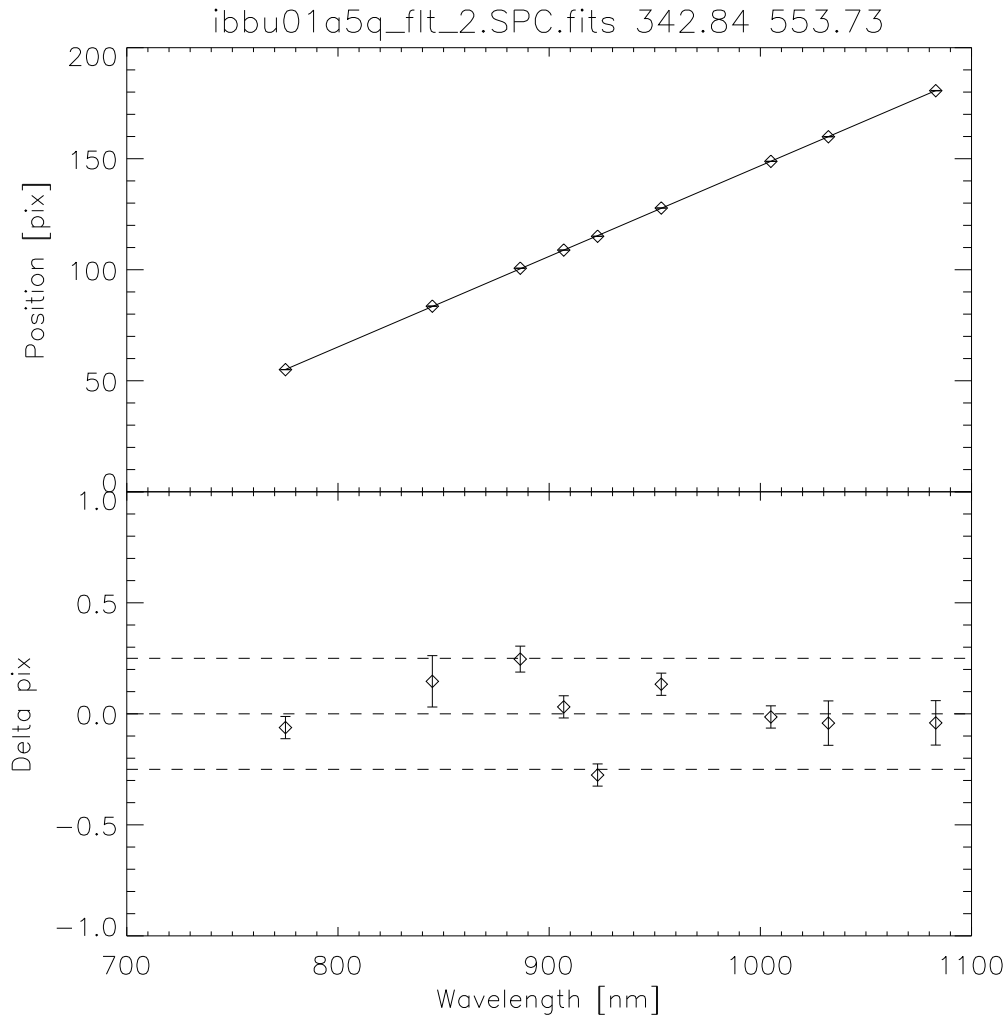


*Figure 5: Linear fit for the wavelength solution of the G102 grism. The example shows a fit to one of the central pointings ( $X_{ref}=342.84$ ,  $Y_{ref}=553.73$ ). The top plot shows the fit whereas the bottom panel shows the deviations from the linear fit; the dashed lines indicate  $\pm 0.25$  pixel deviation from the fit.*

A similar procedure was used to establish wavelength solutions for the +2<sup>nd</sup>, +3<sup>rd</sup> and -1<sup>st</sup> orders of the G102 grism. Due to the limited detector size and therefore reduced wavelength coverage for the higher orders a reduced number of emission lines was used in the fits. The average dispersion per pixel in the higher orders is higher by the approximate ratio of the orders. It is 12.4, 8.2 and -25.1 Å/pix for the +2<sup>nd</sup>, +3<sup>rd</sup>, and -1<sup>st</sup> order, respectively.

Following the methodology used for the trace calibrations we established field

dependent (2-dimensional) fits for the wavelength solution (see Figure 6 and Table 5). The fit shows a marked trend of the wavelength zeropoint with  $X_{\text{ref}}$  position. A trend with  $Y_{\text{ref}}$  position was not significant and thus set to 0.0. The zeropoint measurements show an rms scatter of about 6 Å with respect to the fit. For the dispersion we find a marked trend with  $Y_{\text{ref}}$  position and a much weaker trend with  $X_{\text{ref}}$  positions. The dispersion varies from 23.5 to 25.0 Å/pixel across the full field of view. The measurements show a rms scatter of 0.033 Å/pixel with respect to the fit.

Compared to the ground calibration measurements in TV3 we find a significant change as detailed in Table 4 for a source position at  $X_{\text{ref}}=340$  and  $Y_{\text{ref}}=550$ . However, over most of the wavelength range of the G102 grism the differences are less than one pixel in dispersion direction. The differences are possibly caused by gravity release.

**Table 4: Wavelength solution comparison between TV3 and SMOV for a source at  $X_{\text{ref}}=340$  and  $Y_{\text{ref}}=550$ .**

|      | Zeropoint [Å] | Dispersion [Å/pixel] |
|------|---------------|----------------------|
| TV3  | 6377.4        | 24.692               |
| SMOV | 6402.9        | 24.485               |

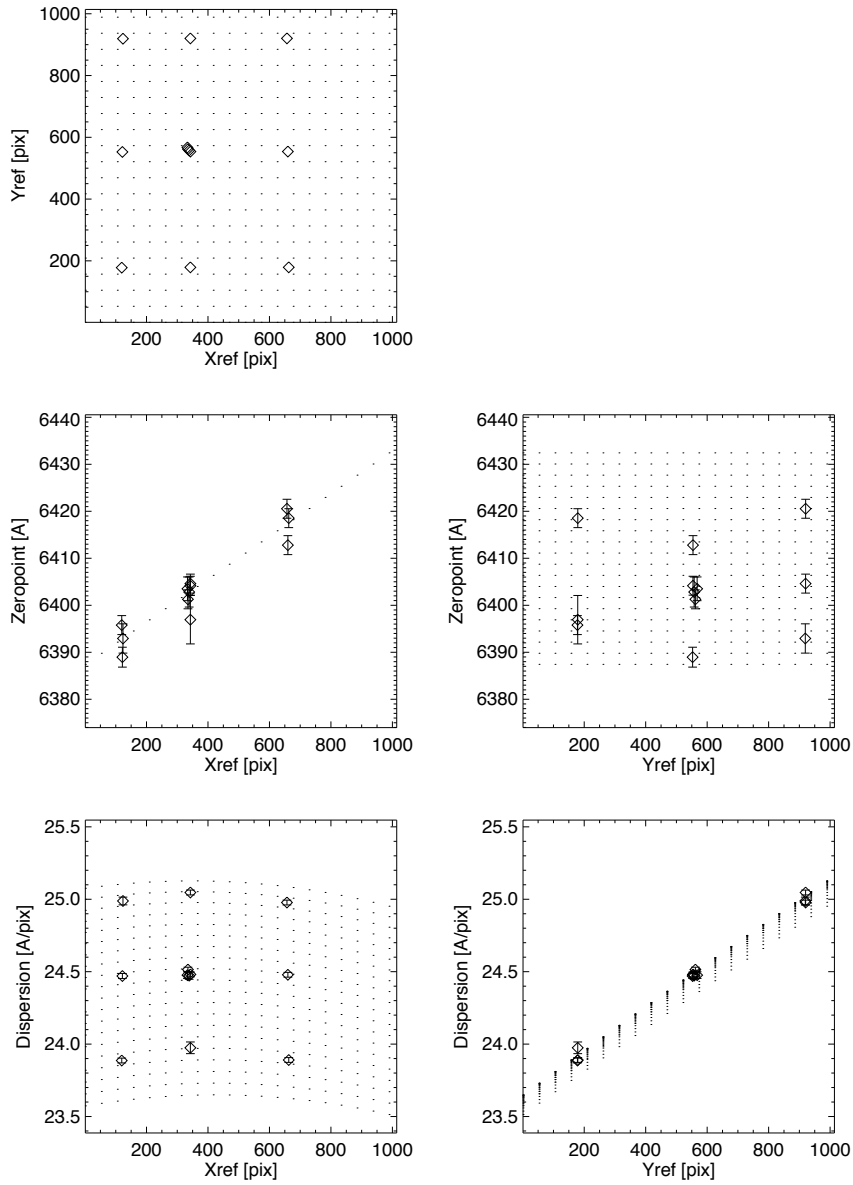


Figure 6: The wavelength solution for the  $G102$  1<sup>st</sup> order spectra is shown as a function of  $X_{ref}$  and  $Y_{ref}$  position (diamond symbols). The final field-dependent wavelength solution (see also Table 5) is shown as the grid of black dots.

**Table 5: Field dependent wavelength solution for G102. Where available errors are given below the values**

| Term                         | a0           | a1(X)        | a2(Y)        | a3(X^2)      | a4(X*Y)      |
|------------------------------|--------------|--------------|--------------|--------------|--------------|
| <b>+1<sup>st</sup> order</b> |              |              |              |              |              |
| DLDP_A_0                     | 6.38738E+03  | 4.55507E-02  | 0.00000E+00  | -            | -            |
| error                        | 3.17621E+00  | 3.19685E-03  | -            | -            | -            |
| DLDP_A_1                     | 2.35716E+01  | 3.60396E-04  | 1.58739E-03  | -4.25234E-07 | -6.53726E-08 |
| error                        | 2.33411E-02  | 1.49194E-04  | 1.05015E-04  | 1.80775E-07  | 9.35939E-08  |
| <b>0<sup>th</sup> order</b>  |              |              |              |              |              |
| DLDP_B_0                     | 8.43577E+03  | -1.33140E+00 | 5.24459E-01  | -            | -            |
| DLDP_B_1                     | 1.37074E+03  | -5.59241E-01 | 5.32039E-01  | -            | -            |
| <b>+2<sup>nd</sup> order</b> |              |              |              |              |              |
| DLDP_C_0                     | 3.22515E+03  | 7.88119E-02  | 0.0          | -            | -            |
| error                        | 3.38678E+00  | 6.07099E-03  | -            | -            | -            |
| DLDP_C_1                     | 1.20099E+01  | -1.47746E-04 | 7.38235E-04  | -            | -            |
| error                        | 6.45984E-03  | 1.14442E-05  | 4.78526E-06  | -            | -            |
| <b>+3<sup>rd</sup> order</b> |              |              |              |              |              |
| DLDP_D_0                     | 2.17651E+03  | 0.0          | 5.01084E-02  | -            | -            |
| error                        | 3.29175E+01  | -            | 7.26124E-02  | -            | -            |
| DLDP_D_1                     | 8.00453E+00  | 0.0          | 4.28339E-04  | -            | -            |
| error                        | 3.70773E-02  | -            | 8.49093E-05  | -            | -            |
| <b>-1<sup>st</sup> order</b> |              |              |              |              |              |
| DLDP_E_0                     | -6.34405E+03 | 0.0          | -1.37004E-01 | -            | -            |
| error                        | 2.67945E+01  | -            | 6.84672E-02  | -            | -            |
| DLDP_E_1                     | -2.42424E+01 | 0.0          | -1.72007E-03 | -            | -            |
| error                        | 4.09626E-02  | -            | 9.44239E-07  | -            | -            |

In Figure 7 we show the individual emission lines of Vy2-2 after the flux calibration (see Section 3.3) and our field-dependent trace and wavelength solutions have been applied to the data. Overall, the field dependent calibrations provide a satisfactory result.

A further test of our in-orbit wavelength calibrations was performed by making use of the flux standard star GD153 (see also Section 3.3). The G102 grism covers the wavelength of the prominent Hydrogen Paschen series lines H P7 (1004.7 nm) and H P6 (1082.8 nm), which are clearly seen in the white dwarf GD153. Using the direct pixel fitting code ppxf (Cappellari & Emsellem 2004) we fit a model spectrum of GD153 (CALSPEC library; gd153\_mod\_005.fits) to the observed spectrum. The ppxf IDL routine involves the logarithmic rebinning of the spectrum and we chose a value of 700 km/s/pixel. We measure a relative velocity between our observations and the model spectrum of  $-49 \pm 57$  km/s, which corresponds to  $0.07 \pm 0.08$  velocity pixels. The above numbers indicate an accuracy of the wavelength zeropoint of  $< 0.25$  pixel. From the fitting procedure we can also

provide a rough estimate of the spectral resolution at the wavelength of the two Paschen lines and obtain  $R=154\pm 22$  at 1040 nm or a FWHM of  $68\pm 10$  Å. This is lower than what would be inferred from the cross-dispersion profile (see Figure 13); further analysis is needed to obtain better estimates on the spectral resolution.

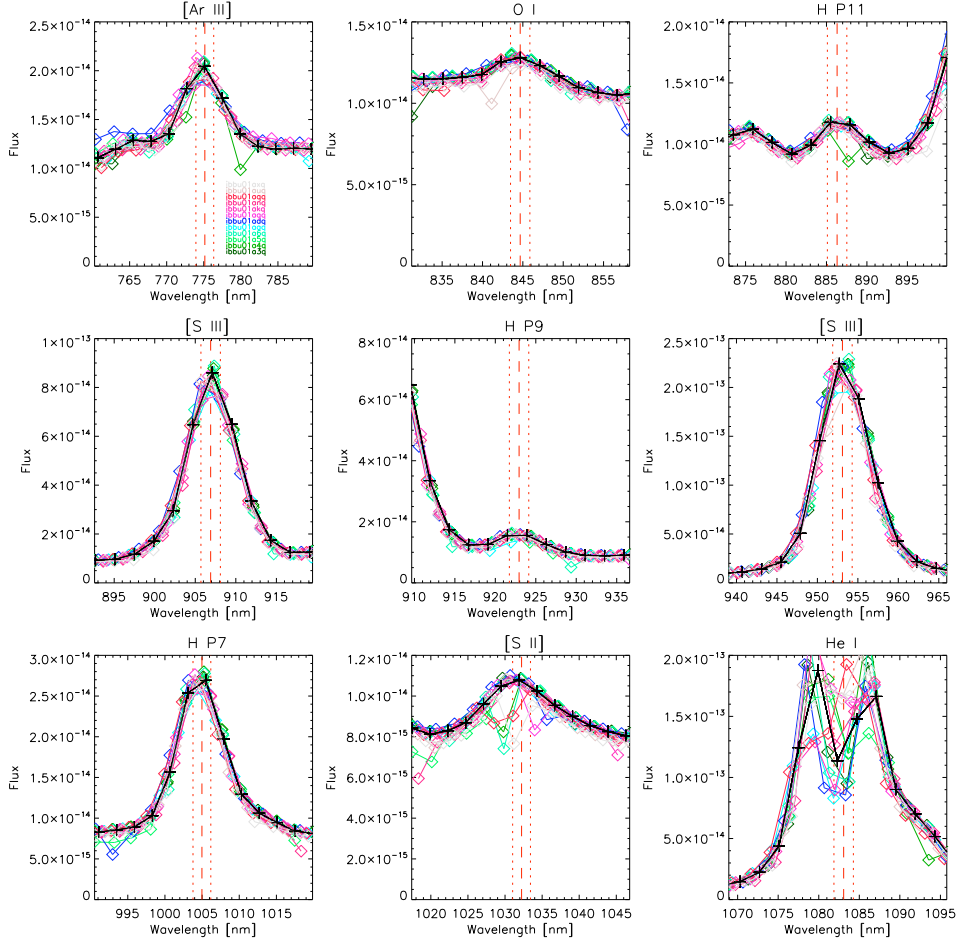


Figure 7: Selected emission lines in the spectra of VY2-2. The aXe software was used to extract the spectra utilizing our field-dependent trace and wavelength solutions established in Section 3.1 and 3.2. Shown in color are the 12 individual spectra covering 9 spatial pointings (see also Figure 1). The 4 central spectra were combined and are shown in black. The color-coding is given in the top left panel. For each panel and emission line we give the identification of the lines in the title and the central wavelength and  $\pm 0.5$  pixel offsets are given as vertical red lines. The central pixels of the He I line (bottom right panel) are saturated and therefore the line appears to have a dip at the center.



### 3.4. Throughput measurements

Using the trace and wavelength solutions derived in the previous sections, the spectra of the flux standard star GD153 observed in Proposal 11552 were extracted. Note, that we make use of our own flat-field calibrations for the G102 grism, which significantly improve the quality of the spectra. There were four, slightly dithered, G102 exposures taken near the central position of the FoV. A further two exposures cover the top left and bottom right corners of the FoV (see Figure 1 and Table A1). For the flux calibration we combine the +1<sup>st</sup> order of the four central exposures into a single spectrum with the help of the spectral drizzle option in the aXe software (aXedrizzle). This spectrum is used to establish the flux calibration for the G102 grism.

Firstly, the spectrum was converted to units of [ $e^- / \text{\AA} / \text{sec}$ ] and divided by a smoothed version of the model spectrum taken from the HST CALSPEC library (gd153\_mod\_005.fits). Smoothing in a sliding 7 pixel window provides the final sensitivity function. The error is evaluated by taking the standard deviation of the four individual sensitivity curves from the central pointings at each wavelength bin and imposing a minimum error of 1%. Using this new sensitivity curve, Figure 8 shows (from the top) the aXe-extracted spectra in electrons per second per pixel, in flux units and the ratio of the observed flux over the model spectrum versus wavelength. In the top plot of Figure 8, significant variations between spectra can be seen since the spectral dispersion ( $\text{\AA}/\text{pixel}$ ) changes as a function of position within the field-of-view. The overall agreement between the fully calibrated standard star spectra (middle plot) is good for the wavelength range 800 to 1120 nm. We note, that the two spectra which show 4-5% less flux are the ones located at the upper left and lower right positions of the FoV. This is clear evidence for a large-scale illumination variation which still requires correction in the grism flat-field cubes. Observations of the flux standard star GD71 in the Cycle 17 calibration program cover 9 pointings over the FoV and will enable such corrections.

Sensitivity curves were also derived for the 0<sup>th</sup>, +2<sup>nd</sup>, +3<sup>rd</sup> and -1<sup>st</sup> orders. For the +2<sup>nd</sup> order we combined the 4 central exposures, whereas for the +3<sup>rd</sup> and -1<sup>st</sup> orders only one exposure was available. In Figure 9 we summarize the results for all sensitivity curves. Compared to the TV3 results we find up to 10% more throughput in the +1<sup>st</sup> order. The TV3 results are shown as green lines in Figure 9.

The peak throughput of HST + WFC3 G102 is 41.8% at 1100 nm while it is >10% over the wavelength range 800 to 1150 nm.

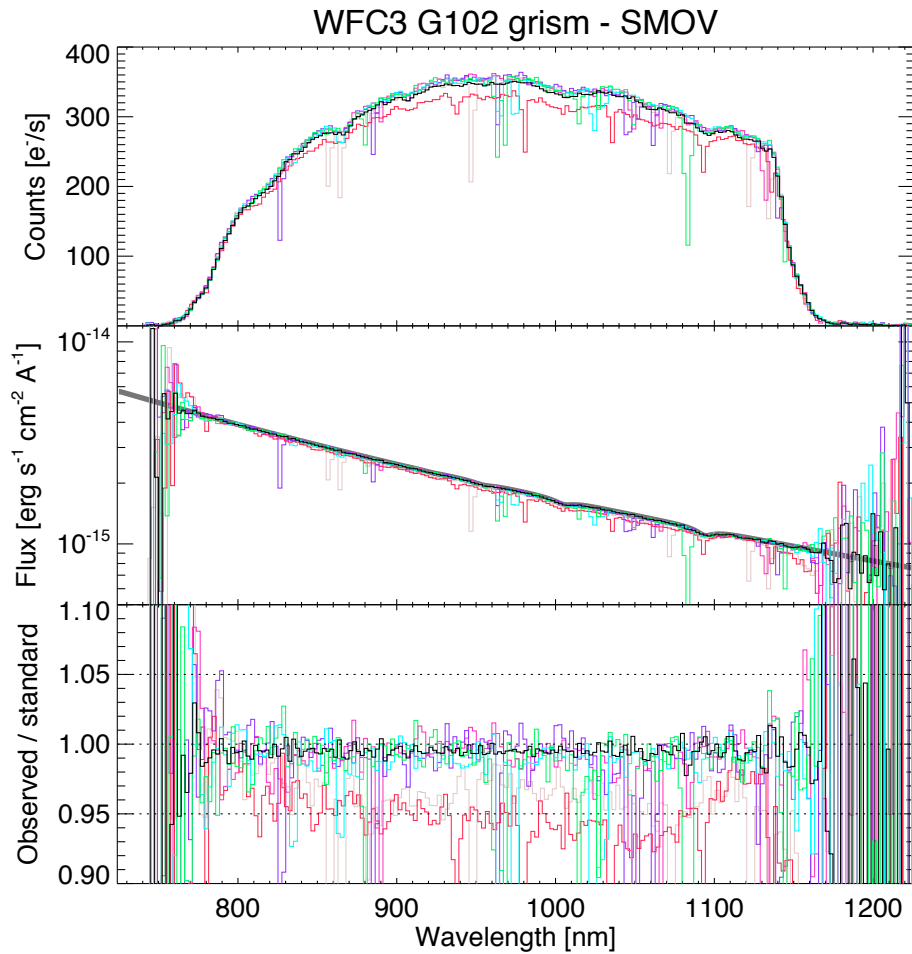
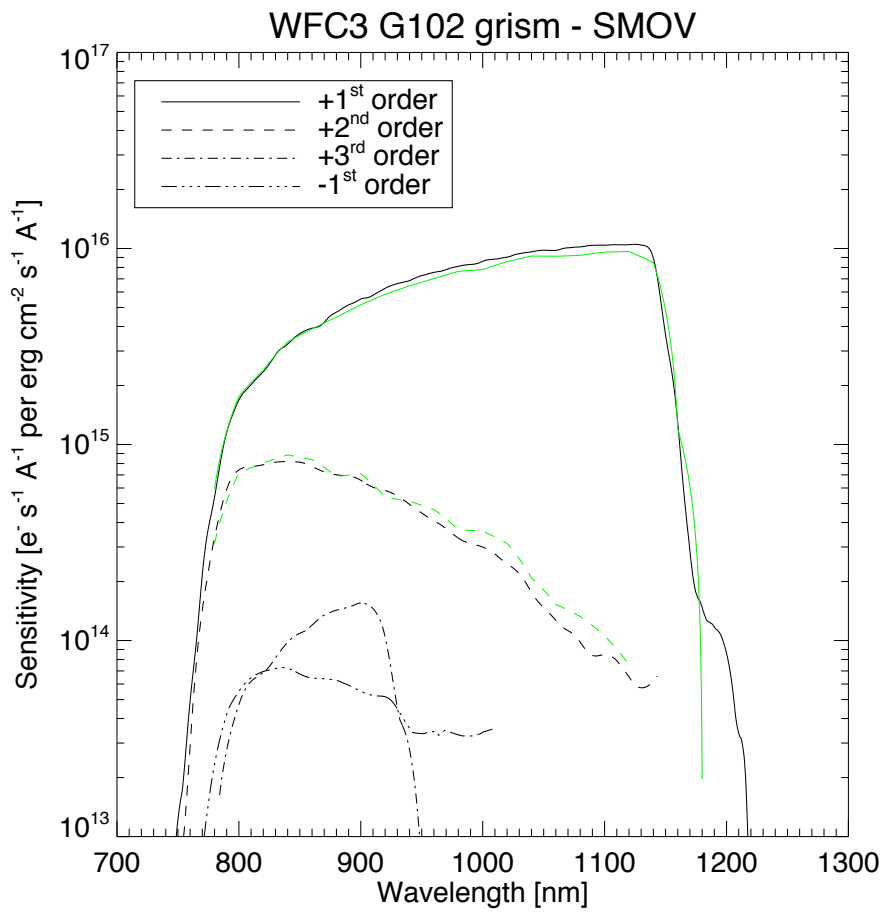


Figure 8: The *aXe* extracted 1-dimensional spectra of the standard star GD153 in units of electrons per second per pixel, fully calibrated flux units and the ratio of the observed flux over the model spectrum versus wavelength (from top to bottom). Observations obtained at different field positions are colored, and the combined (*aXedrizzle*) central spectrum is shown in black. In the individually extracted spectra there are a number of prominent wavelength steps, which show too low flux. These points are caused by pixels, which are flagged in the original *flt* files. The *aXedrizzle* spectrum corrects for these effects and thus does not show any deviant wavelength steps.



*Figure 9: Sensitivities of the G102 grism for the +1<sup>st</sup>, +2<sup>nd</sup>, +3<sup>rd</sup> and -1<sup>st</sup> orders. The results were derived from the observations of the flux standard GD153 during SMOV (Proposal 11552). For comparison we show in green the measurements obtained during the TV3 ground calibrations.*

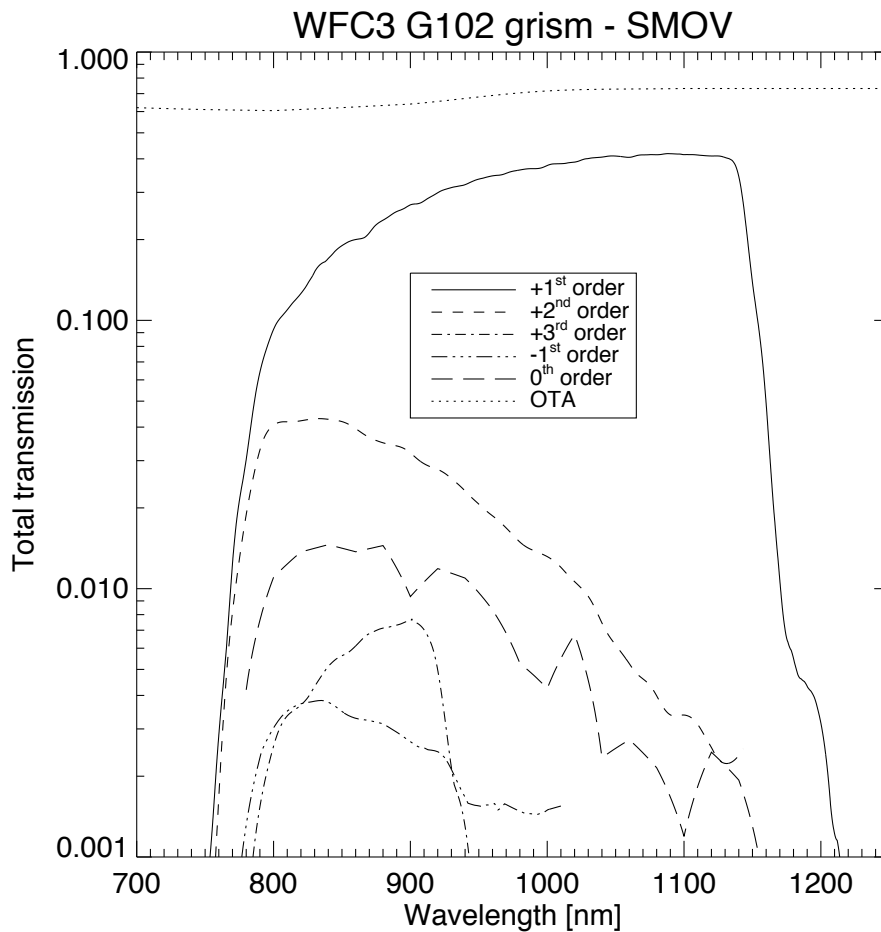


Figure 10: Total throughput estimates for the +1<sup>st</sup>, +2<sup>nd</sup>, +3<sup>rd</sup> and -1<sup>st</sup> orders of the G102 grism, derived from the sensitivity curves of this report. The 0<sup>th</sup> order is taken from the TV3 ground calibrations and only shown for comparison.

In Figure 11 we compare the total throughput estimates from the WFC3 IR grisms with “synphot” predictions. The synphot files are based and calibrated to WFC3 imaging from the SMOV observations. The plot shows theoretical values, which would be achieved with WFC3 without any filter or grism inserted. The analysis of the G141 grism is described in detail in Kuntschner et al. (2008a, b). The overall agreement to better than  $\pm 5\%$  is good and shows that a consistent first order flux calibration of the IR channel was achieved.

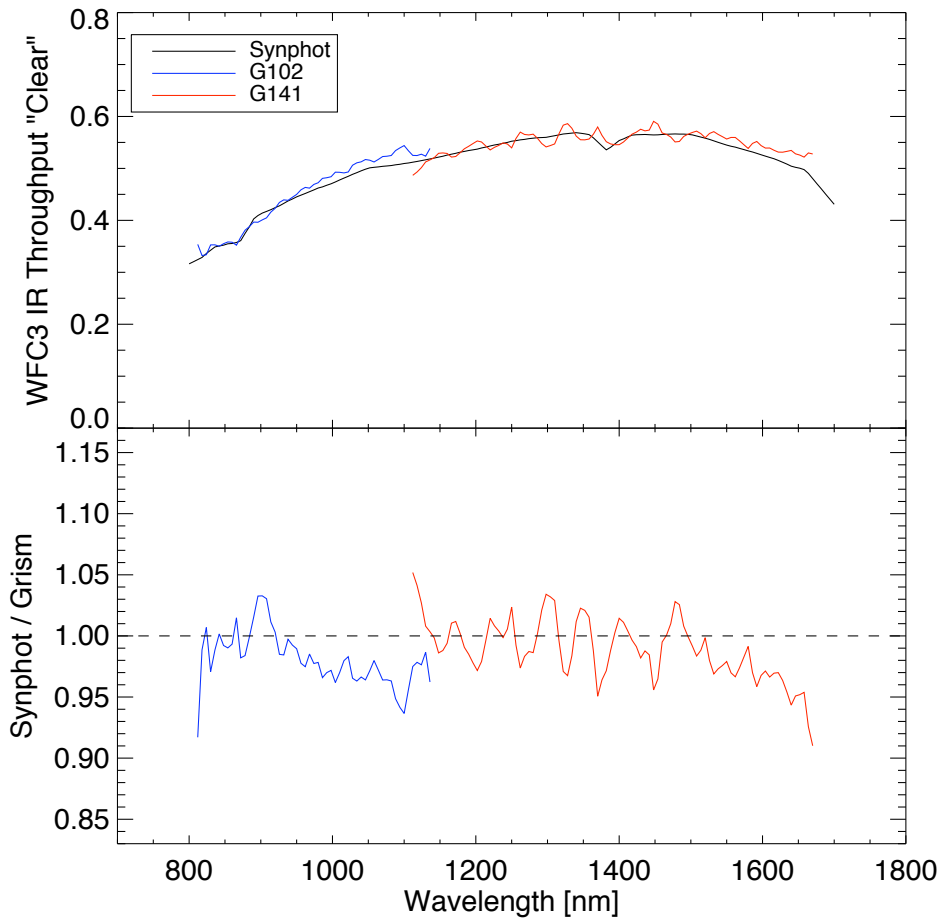


Figure 11: Comparison of total throughput “synphot” predictions with SMOV observations of the WFC3 IR grisms. The upper plot shows theoretical values, which would be achieved with WFC3 without any filter or grism inserted. The lower plot shows the ratio of Synphot predictions over observations.

### 3.5. Aperture corrections and cross dispersion PSF

Using the aXe software (aXedrizzle option) we derived a rectified 2-dimensional image for the central exposures of the flux standard star GD153. The resulting image (called “stamp” image) is wavelength calibrated and image distortions, as recorded in our trace calibrations, are removed. From this image, covering a 220 pixel wide aperture around GD153, various sub-apertures (here used in the sense of

a diameter) are extracted with the help of IDL scripts and compared to the flux one determines in the largest aperture. This procedure is carried out as a function of wavelength in five bins. The resulting aperture correction values are given in Tables 6 and shown in Figure 12. About 95% of the flux is concentrated in an aperture of 11 pixels diameter or 1.411 arcsec.

The aperture corrections derived from in orbit data compare well with TV3 results with a maximum difference of 3%.

**Table 6: Aperture corrections for WFC3 G102**

| Diameter<br>[arcsec] | 8850 Å | 9350 Å | 9850 Å | 10350 Å | 10850 Å | 11350 Å |
|----------------------|--------|--------|--------|---------|---------|---------|
| 0.128                | 0.466  | 0.392  | 0.415  | 0.468   | 0.422   | 0.372   |
| 0.385                | 0.826  | 0.810  | 0.808  | 0.816   | 0.789   | 0.795   |
| 0.641                | 0.891  | 0.889  | 0.889  | 0.886   | 0.868   | 0.890   |
| 0.898                | 0.921  | 0.918  | 0.918  | 0.914   | 0.896   | 0.918   |
| 1.154                | 0.939  | 0.938  | 0.938  | 0.934   | 0.918   | 0.938   |
| 1.411                | 0.952  | 0.951  | 0.952  | 0.948   | 0.932   | 0.951   |
| 1.667                | 0.962  | 0.962  | 0.963  | 0.959   | 0.943   | 0.960   |
| 1.924                | 0.969  | 0.969  | 0.970  | 0.967   | 0.952   | 0.967   |
| 3.719                | 0.984  | 0.985  | 0.988  | 0.986   | 0.973   | 0.985   |
| 7.567                | 0.993  | 0.996  | 0.998  | 0.996   | 0.986   | 0.995   |
| 12.954               | 0.998  | 0.999  | 0.999  | 0.999   | 0.992   | 0.998   |
| 25.779               | 1.000  | 1.000  | 1.000  | 1.000   | 1.000   | 1.000   |

## WFC3/IR G102 SMOV Aper corr center

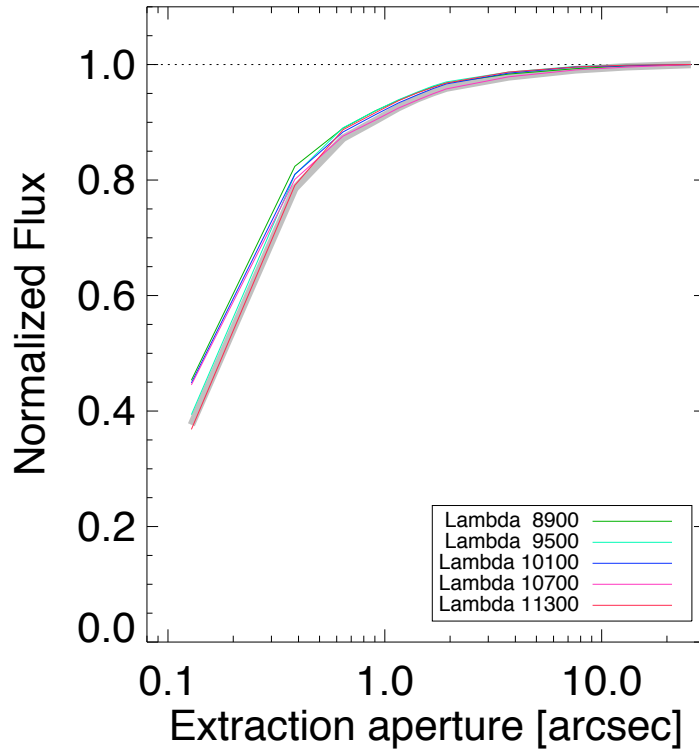


Figure 12: Aperture corrections for WFC3 G102 as a function of aperture (=diameter) and wavelength. For comparison TV3 data at 985 nm is shown as thick grey line.

We also investigated the cross dispersion PSF of the central pointing for the flux standard star GD153. Ground calibration results showed that the G102 grism produces, for a Gaussian approximation, a cross dispersion width (FWHM) of 1.3 to 1.4 pixel (see Kuntschner et al. 2009). We show in Figure 13 the SMOV measurements, which indicate a slightly smaller width in comparison with TV3 results. Sampling effects cause the wave like structure of the measurements and we consider the minima as good representations of the true cross dispersion PSF. The measurements are also in agreement with the expectations from the direct imaging also shown in Figure 13. In conclusion, the G102 grism is in focus and produces spectra of point sources in agreement with design expectations.

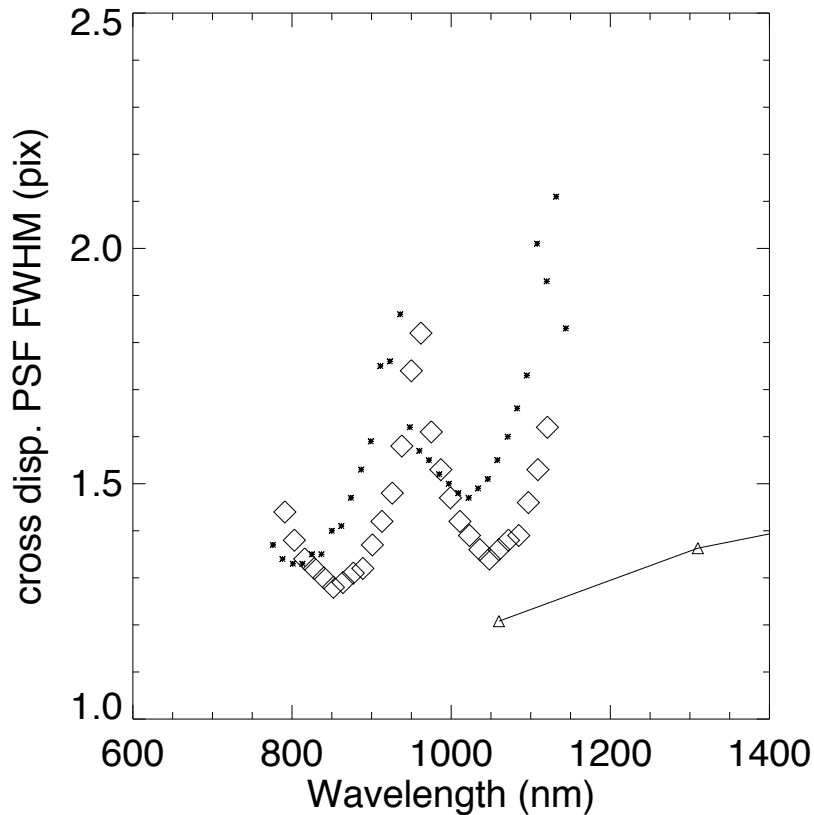


Figure 13: Cross-dispersion profile width as measured in FWHM (pixel) for a Gaussian approximation. Diamonds represent the SMOV data for one of the central pointings for grism G102. The small stars show estimates derived from white light images obtained during the TV3 ground calibrations (see Kuntzschner et al. 2009). The triangles connected with a solid line show for comparison measurements from the TV3 direct light images as tabulated by Hartig (2008b).

## 4. Conclusions

This ISR presented the calibration of the WFC3 G102 grism based on SMOV data and one Cycle 17 wavelength calibration proposal. We have established in-orbit, source position dependent calibrations of the trace and wavelength solution for the +1<sup>st</sup> order “science” spectra. Both, the local trace and wavelength solution can be approximated with a linear solution. The mean dispersion of the G102 grism is 24.5 Å/pixel varying from 23.5 to 25.0 Å/pixel across the field of view. The in-



orbit solutions agree well ( $\leq 1$  pixel) with the calibrations established during ground calibrations in TV2 and TV3. We also provide, field dependent calibrations for the +2<sup>nd</sup>, +3<sup>rd</sup> and -1<sup>st</sup> spectral orders, albeit with a less rigorous analysis.

We establish flux calibrations for the +1<sup>st</sup>, +2<sup>nd</sup> +3<sup>rd</sup> and -1<sup>st</sup> orders. Furthermore, we provide aperture corrections for the +1<sup>st</sup> order as a function of wavelength. The throughput of HST + WGC3 G102 peaks at 11000 Å with 41.8% and is above 10% between 8000 and 11500 Å.

## Appendix

The datasets acquired during SMOV Proposal 11552 (PI Bushouse) and the Cycle 17 calibration program of Proposal 11937 (PI Bushouse) are listed in Table A1 and A2, respectively. Note, that throughout this report we use the name of “HB12” for the target PN G111.8-02.8.

**Table A1. Summary of observations for the calibration of the grism G102 in Proposal 11552**

| FILE      | TARGNAME       | FILTER | EXPTIME<br>[seconds] | POSTARG1<br>[arcsec] | POSTARG2<br>[arcsec] |
|-----------|----------------|--------|----------------------|----------------------|----------------------|
| iab901eiq | GD-153         | F098M  | 5.86                 | -20.0                | 0.0                  |
| iab901ejq | GD-153         | F105W  | 2.93                 | -20.0                | 0.0                  |
| iab901ekq | GD-153         | G102   | 102.93               | -20.0                | 0.0                  |
| iab901elq | GD-153         | G102   | 102.93               | -20.5                | 0.5                  |
| iab901emq | GD-153         | G102   | 102.93               | -21.0                | 1.0                  |
| iab901enq | GD-153         | G102   | 102.93               | -21.2                | 1.2                  |
| iab901eqq | GD-153         | F098M  | 5.86                 | 23.0                 | -45.0                |
| iab901erq | GD-153         | F105W  | 2.93                 | 23.0                 | -45.0                |
| iab901esq | GD-153         | G102   | 102.93               | 23.0                 | -45.0                |
| iab9a1ewq | GD-153         | F098M  | 5.86                 | -50.0                | 45.0                 |
| iab9a1exq | GD-153         | F105W  | 2.93                 | -50.0                | 45.0                 |
| iab9a1eyq | GD-153         | G102   | 102.93               | -50.0                | 45.0                 |
|           |                |        |                      |                      |                      |
| iab907j5q | PN-G111.8-02.8 | F098M  | 2.93                 | -20.0                | 0.0                  |
| iab907j6q | PN-G111.8-02.8 | G102   | 102.93               | -20.0                | 0.0                  |
| iab907j9q | PN-G111.8-02.8 | F098M  | 2.93                 | -50.0                | 45.0                 |
| iab907jaq | PN-G111.8-02.8 | G102   | 102.93               | -50.0                | 45.0                 |
| iab907jbq | PN-G111.8-02.8 | F098M  | 2.93                 | -20.0                | 45.0                 |
| iab907jcq | PN-G111.8-02.8 | G102   | 102.93               | -20.0                | 45.0                 |
| iab907jdq | PN-G111.8-02.8 | F098M  | 2.93                 | 23.0                 | 45.0                 |
| iab907jeq | PN-G111.8-02.8 | G102   | 102.93               | -23.0                | -45.0                |

ST-ECF Technical Instrument Report WFC3-2009-18

|           |                |       |        |       |       |
|-----------|----------------|-------|--------|-------|-------|
| iab907jfq | PN-G111.8-02.8 | F098M | 2.93   | -50.0 | 0.0   |
| iab907jgq | PN-G111.8-02.8 | G102  | 102.93 | -50.0 | 0.0   |
| iab907jhq | PN-G111.8-02.8 | F098M | 2.93   | 23.0  | 0.0   |
| iab907jiq | PN-G111.8-02.8 | G102  | 102.93 | 23.0  | 0.0   |
| iab907jkq | PN-G111.8-02.8 | F098M | 2.93   | -50.0 | -45.0 |
| iab907jlq | PN-G111.8-02.8 | G102  | 102.93 | -50.0 | -45.0 |
| iab907jmq | PN-G111.8-02.8 | F098M | 2.93   | -20.0 | -45.0 |
| iab907jng | PN-G111.8-02.8 | G102  | 102.93 | -20.0 | -45.0 |
| iab907joq | PN-G111.8-02.8 | F098M | 2.93   | 23.0  | -45.0 |
| iab907jpq | PN-G111.8-02.8 | G102  | 102.93 | 23.0  | -45.0 |

**Table A1. Summary of observations for the calibration of the grism G102 in Proposal 11937**

| FILE      | TARGNAME | FILTER | EXPTIME<br>[seconds] | POSTARG1<br>[arcsec] | POSTARG2<br>[arcsec] |
|-----------|----------|--------|----------------------|----------------------|----------------------|
| ibbu01a1q | VY2-2    | F098M  | 5.86                 | -20.0                | 0.0                  |
| ibbu01a2q | VY2-2    | F105W  | 2.93                 | -20.0                | 0.0                  |
| ibbu01a3q | VY2-2    | G102   | 102.93               | -20.0                | 0.0                  |
| ibbu01a4q | VY2-2    | G102   | 102.93               | -20.5                | 0.5                  |
| ibbu01a5q | VY2-2    | G102   | 102.93               | -21.0                | 1.0                  |
| ibbu01a6q | VY2-2    | G102   | 102.93               | -21.2                | 1.2                  |
| ibbu01a8q | VY2-2    | F098M  | 5.86                 | -50.0                | 45.0                 |
| ibbu01a9q | VY2-2    | F105W  | 2.93                 | -50.0                | 45.0                 |
| ibbu01aaq | VY2-2    | G102   | 102.93               | -50.0                | 45.0                 |
| ibbu01abq | VY2-2    | F098M  | 5.86                 | -20.0                | 45.0                 |
| ibbu01acq | VY2-2    | F105W  | 2.93                 | -20.0                | 45.0                 |
| ibbu01adq | VY2-2    | G102   | 102.93               | -20.0                | 45.0                 |
| ibbu01aeq | VY2-2    | F098M  | 5.86                 | 23.0                 | 45.0                 |
| ibbu01afq | VY2-2    | F105W  | 2.93                 | 23.0                 | 45.0                 |
| ibbu01agq | VY2-2    | G102   | 102.93               | 23.0                 | 45.0                 |
| ibbu01aiq | VY2-2    | F098M  | 5.86                 | -50.0                | 0.0                  |
| ibbu01ajq | VY2-2    | F105W  | 2.93                 | -50.0                | 0.0                  |
| ibbu01akq | VY2-2    | G102   | 102.93               | -50.0                | 0.0                  |
| ibbu01alq | VY2-2    | F098M  | 5.86                 | 23.0                 | 0.0                  |
| ibbu01amq | VY2-2    | F105W  | 2.93                 | 23.0                 | 0.0                  |
| ibbu01anq | VY2-2    | G102   | 102.93               | 23.0                 | 0.0                  |
| ibbu01aoq | VY2-2    | F098M  | 5.86                 | -50.0                | -45.0                |
| ibbu01apq | VY2-2    | F105W  | 2.93                 | -50.0                | -45.0                |
| ibbu01aqq | VY2-2    | G102   | 102.93               | -50.0                | -45.0                |
| ibbu01asq | VY2-2    | F098M  | 5.86                 | -20.0                | -45.0                |
| ibbu01atq | VY2-2    | F105W  | 2.93                 | -20.0                | -45.0                |
| ibbu01auq | VY2-2    | G102   | 102.93               | -20.0                | -45.0                |

## ST-ECF Technical Instrument Report WFC3-2009-18

|           |       |       |        |      |       |
|-----------|-------|-------|--------|------|-------|
| ibbu01avq | VY2-2 | F098M | 5.86   | 23.0 | -45.0 |
| ibbu01awq | VY2-2 | F105W | 2.93   | 23.0 | -45.0 |
| ibbu01axq | VY2-2 | G102  | 102.93 | 23.0 | -45.0 |

## References

Bertin, E., Arnouts, S. 1996, AAS, 117, 393

Cappellari M., Emsellem E., 2004, PASP, 116, 138

Hora, J. L., Latter, W.B., Deutsch, L. K., 1999, APJS, 124, 195

Kuntschner, H. Bushouse, H., Kümmel, M., Walsh, J. R., 2009, WFC3 Instrument Science Report, WFC3-2009-04: The cross dispersion profiles of the WFC3 grisms

Kuntschner, H. Bushouse, H., Walsh, J. R., Kümmel, M., 2008a, WFC3 Instrument Science Report, WFC3-2008-16: The TV3 ground calibrations of the WFC3 NIR grisms

Kuntschner, H. Bushouse, H., Walsh, J. R., Kümmel, M., 2008b, WFC3 Instrument Science Report, WFC3-2008-15: The TV2 ground calibrations of the WFC3 NIR grisms

Pirzkal, N., Bohlin, R. Thatte, D., 2009, NICMOS Instrument Science Report, NICMOS-2009-006: NICMOS Grism Wavelength Calibration